Solvent-inducted structural diversity of two luminescent metal-organic frameworks as dual-functional sensor for the detection of nitroaromatic compounds and highly selective detection of ofloxacin antibiotics

Xiao-Qiang Yao,*[a,b] Guo-Bin Xiao,[a] Hua Xie,[a] Dong-Dong Qin,[a] Heng-Chang Ma,[a] Jia-Cheng Liu,[a] and Pen-Ji Yan[a, c]

[a]Key Laboratory of Eco-Environment-Related Polymer Materials of Ministry of Education, Key Laboratory of Polymer Materials of Gansu Province, College of Chemistry and Chemical Engineering, Northwest Normal University, Lanzhou 730070, P. R. China

[b]Jiangsu Collaborative Innovation Center of Atmospheric Environment and Equipment Technology (CICAEET), Jiangsu Key Laboratory of Atmospheric Environment Monitoring and Pollution Control (AEMPC), School of Environmental Sciences and Engineering, Nanjing University of Information Science and Technology, Nanjing, 210044, P. R. China.

[c]College of Chemistry and Chemical Engineering, Key Laboratory of Hexi Corridor Resources Utilization of Gansu Universities, Hexi University, Zhangye 734000, P. R. China

* Corresponding author: Xiao-Qiang Yao
E-mail: yxq@nwnu.edu.cn

Contents

nitroaromatic compounds.

Fig. S12 Powder X-ray diffraction patterns of compound **1**, activated, after NB test in DMF and after NB test in DMF five cycles.

Fig. S13 The fluorescence spectra of compound **1** in DMF solution upon the addition of 10^{-2} mol/L of various antibiotics.

Fig. S14 Schematic representation of fluorescence emission and electron-transfer processes.

Fig. S15 HOMO and LUMO energy levels of compound **1** and antibiotics (The energy levels of frontier molecular orbitals were calculated by DFT at the level of B3LYP/6-31G*–SDD).

Fig. S16 The UV-Vis absorption spectra of various antibiotics and the excitation spectra of **1**.

Table S1 Crystallographic Data and Structure Refinement Details for **1** and **2.**

Table S2 Selected bond lengths (Å) and angles (deg) for **1** and **2.**

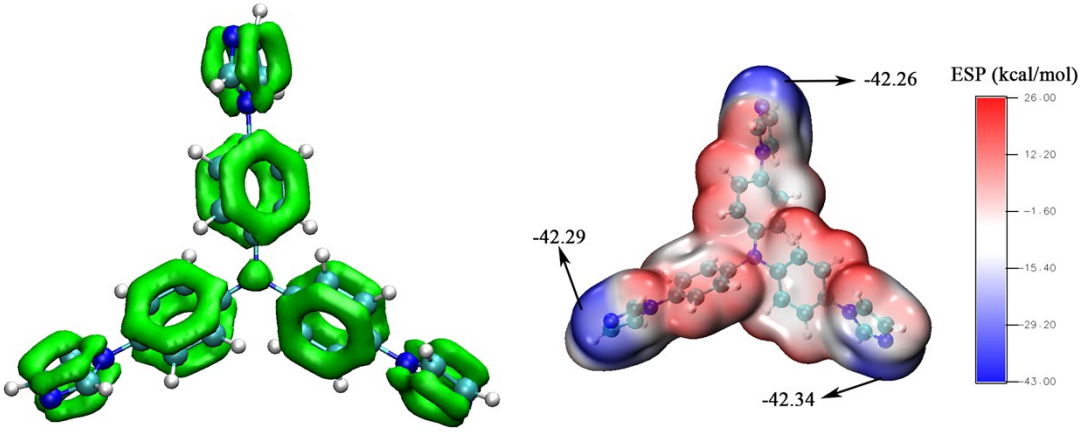

Fig. S1 (left) Schematic illustration of the π-electron rich triangular ligand TIPA. (right) As shown from the electrostatic potential (ESP) of TIPA, the large negative values around the imidazole-N atoms indicate that TIPA has good coordination ability.

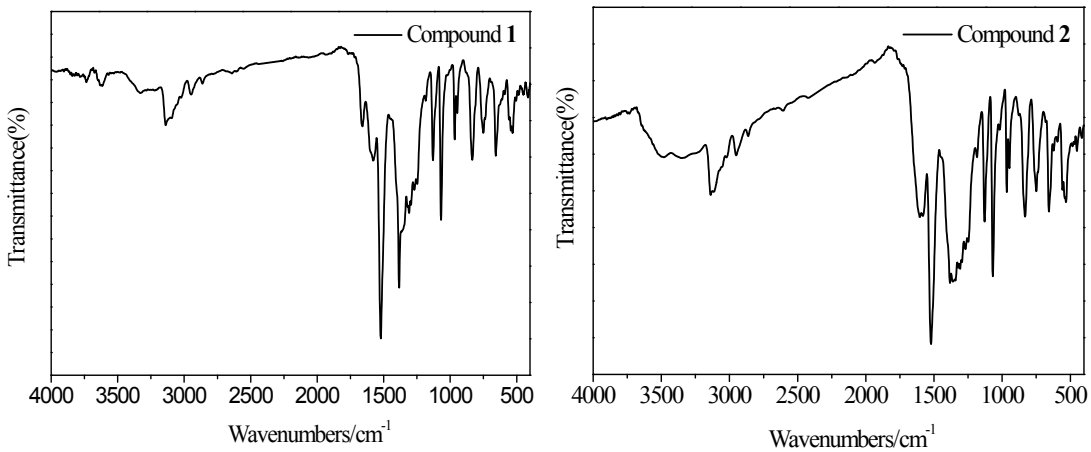

Fig. S2 The FT-IR spectrogram of **1** and **2**.

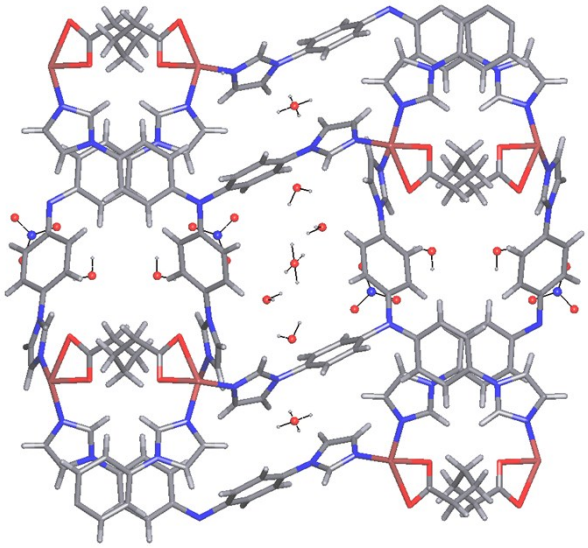

Fig. S3 The channels of **1** are filled with abundant water molecules.

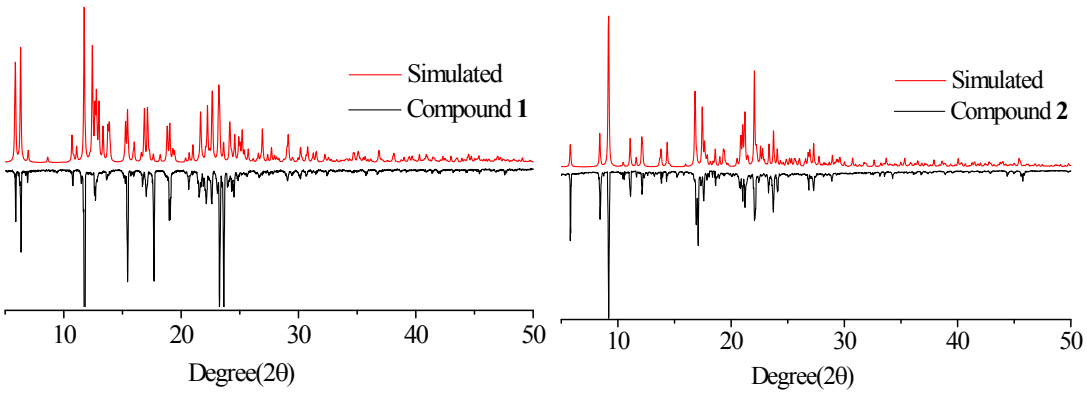

Fig. S4 Powder X-ray diffraction patterns of **1** and **2**.

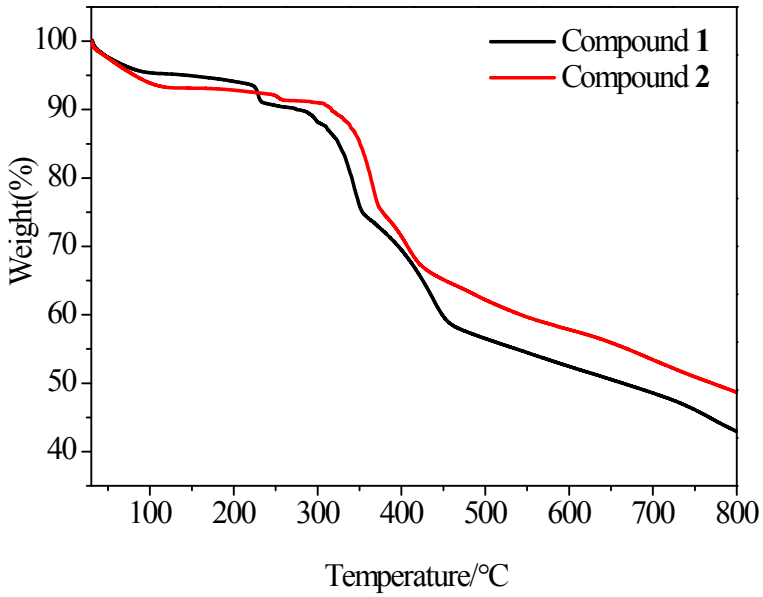

Fig. S5 The TGA curves of **1** and **2**.

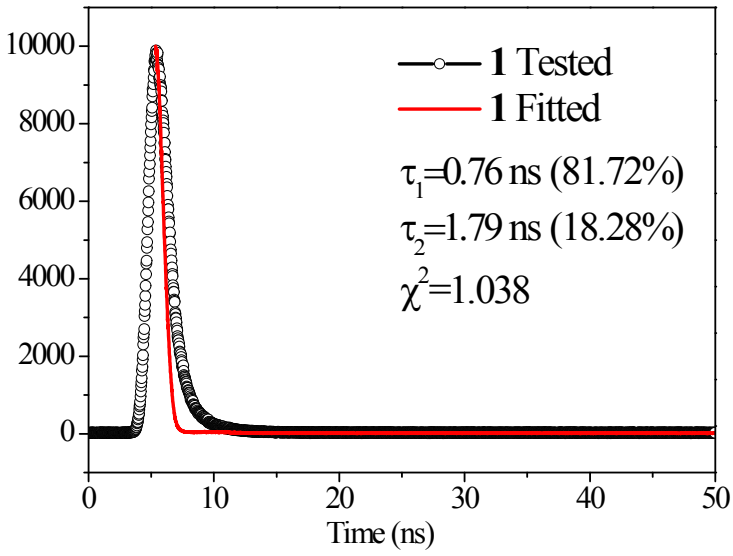

Fig. S6 The luminescence lifetime of **1** in the solid state at room temperature. The average lifetime was analyzed using the following equation: $\tau_{(avg)} = (\alpha_1\tau_1^2 + \alpha_2\tau_2^2) / (\alpha_1\tau_1 + \alpha_2\tau_2)$, where τ is the lifetime and α is the pre-exponential factor with subscripts 1 and 2 representing various species, $\tau_{(avg)} = 1.12$ ns.

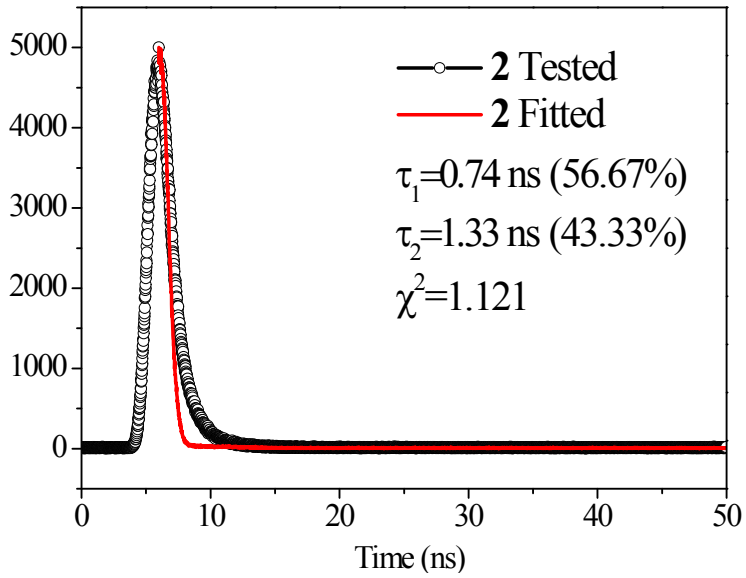

Fig. S7 The luminescence lifetime of **2** in the solid state at room temperature. The average lifetime was analyzed using the following equation: $\tau_{(avg)} = (\alpha_1\tau_1^2 + \alpha_2\tau_2^2) / (\alpha_1\tau_1 + \alpha_2\tau_2)$, where τ is the lifetime and α is the pre-exponential factor with subscripts 1 and 2 representing various species, $\tau_{(avg)} = 1.08$ ns.

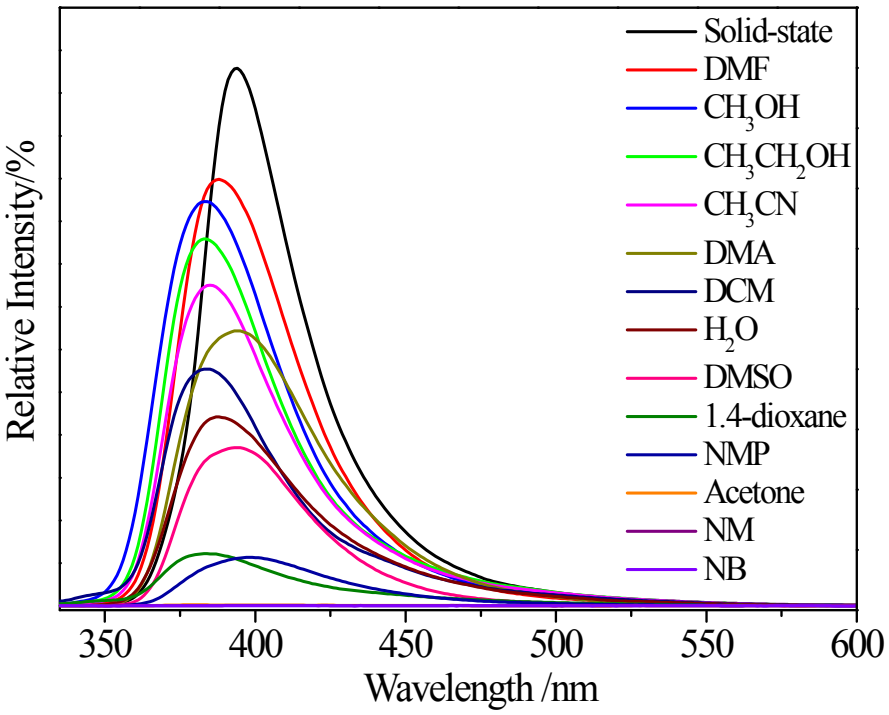

Fig. S8 The emission spectra of **1** in diverse analytes and solid state.

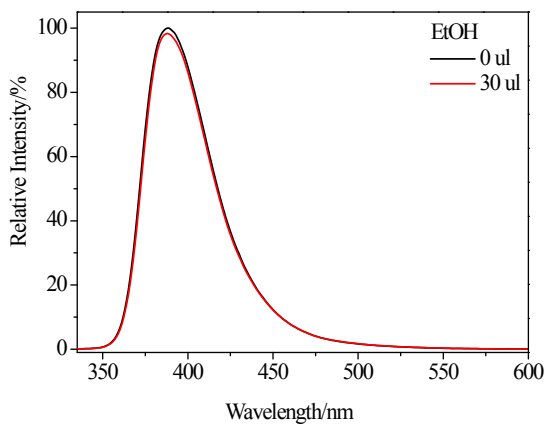
EtOH
0 ul
30 ul
Relative Intensity/%
Wavelength/nm

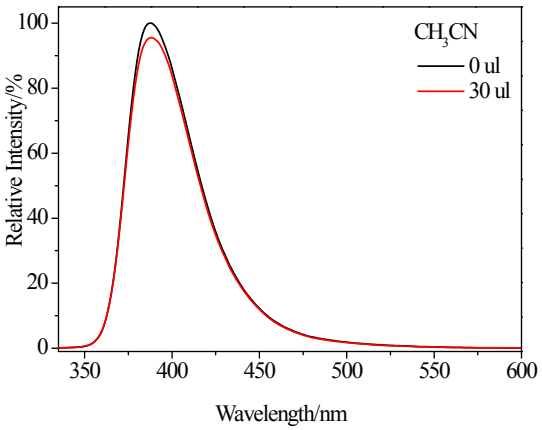
CH3CN
0 ul
30 ul
Relative Intensity/%
Wavelength/nm

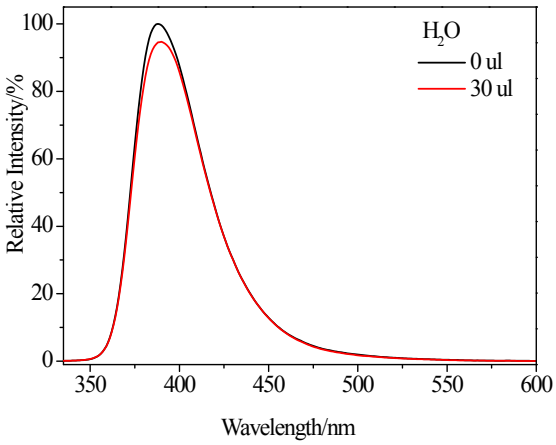
H2O
0 ul
30 ul
Relative Intensity/%
Wavelength/nm

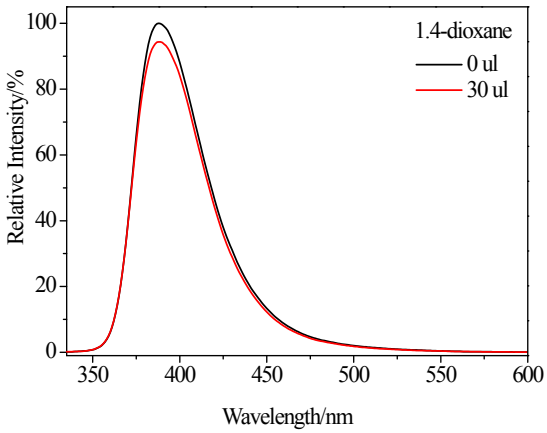
1.4-dioxane
0 ul
30 ul
Relative Intensity/%
Wavelength/nm

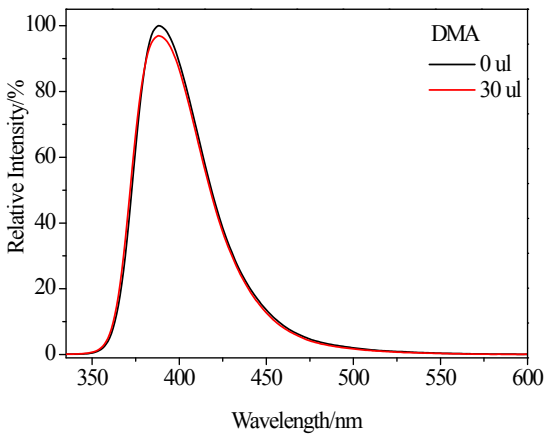
DMA
0 ul
30 ul
Relative Intensity/%
Wavelength/nm

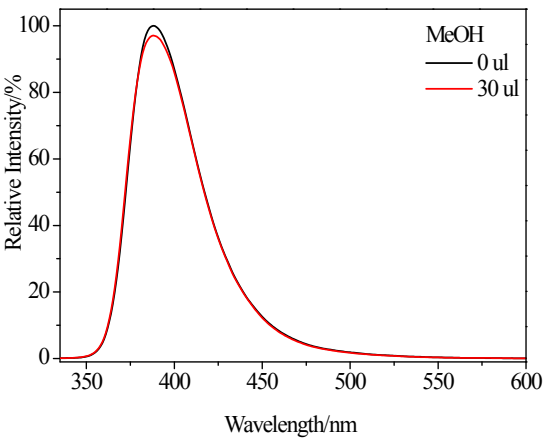
MeOH
0 ul
30 ul
Relative Intensity/%
Wavelength/nm

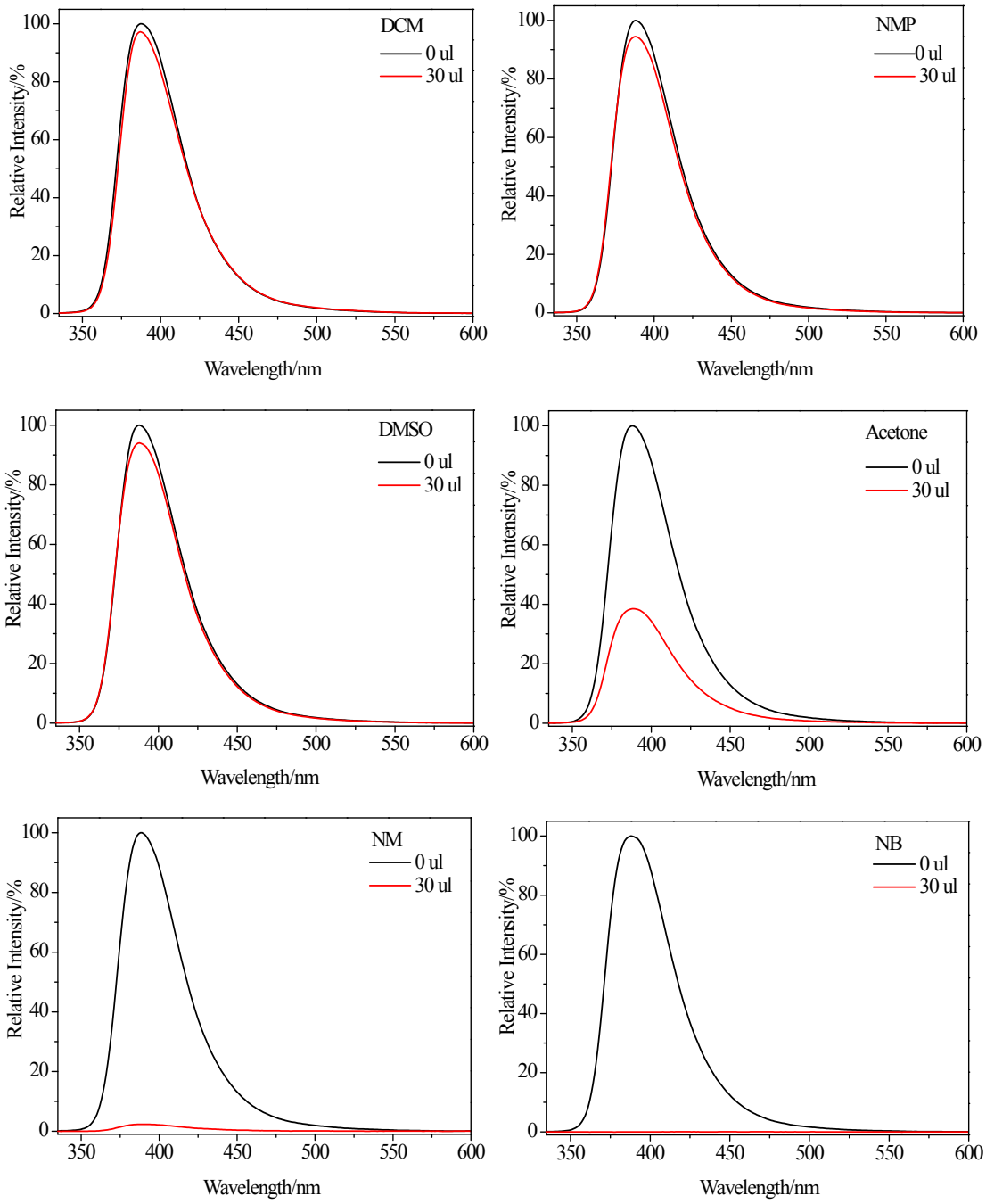

Fig. S9 The fluorescence spectra of compound **1** in DMF solution upon the addition of various solvents.

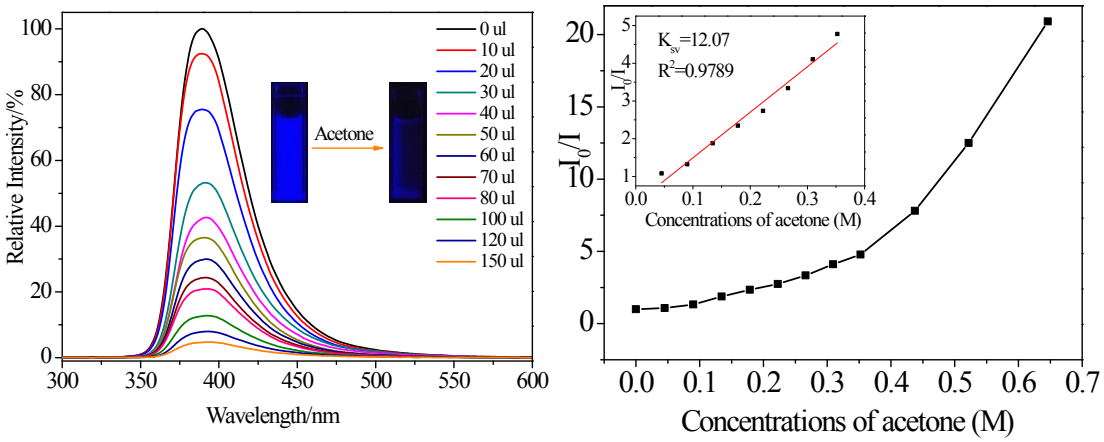

Fig. S10 Photoluminescence spectra and SV curve for **1** by gradual addition of acetone in DMF, the insets demonstrate the quenching linearity relationship at low concentrations of acetone.

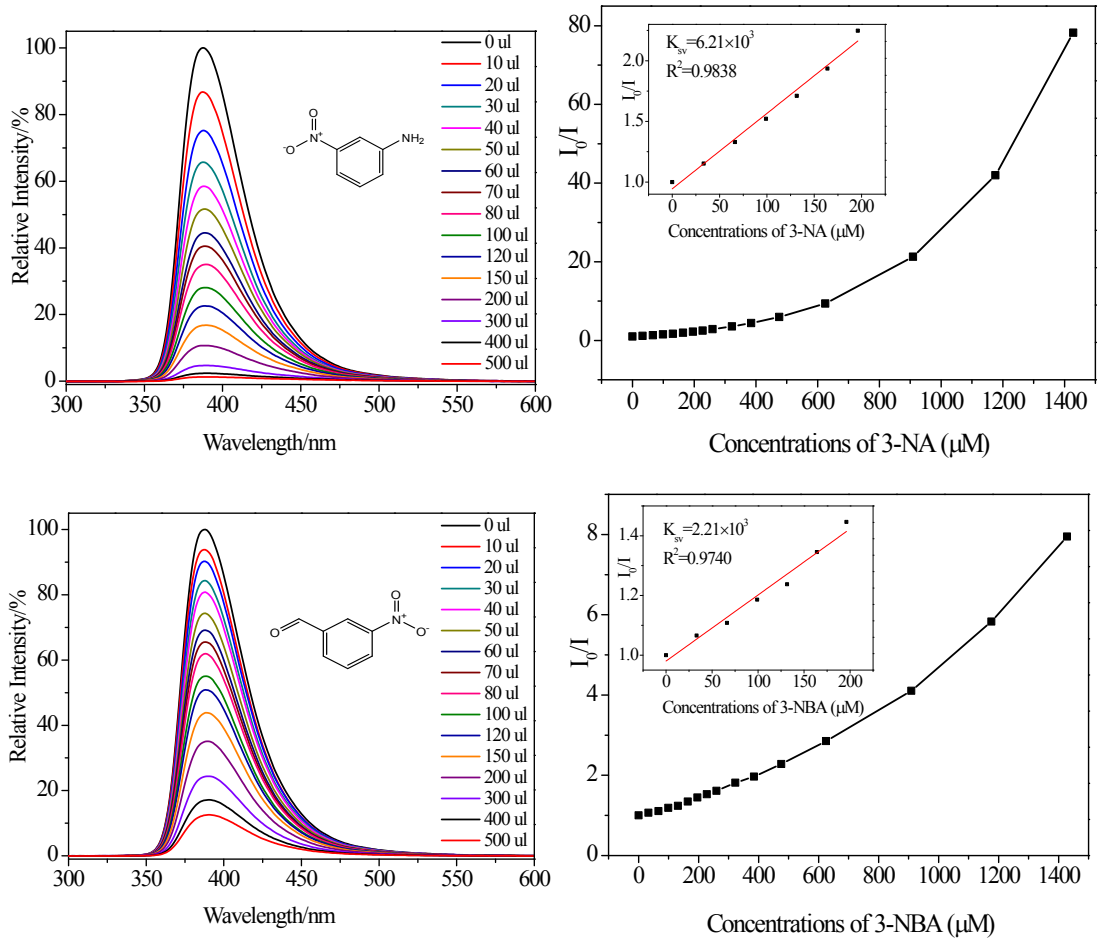

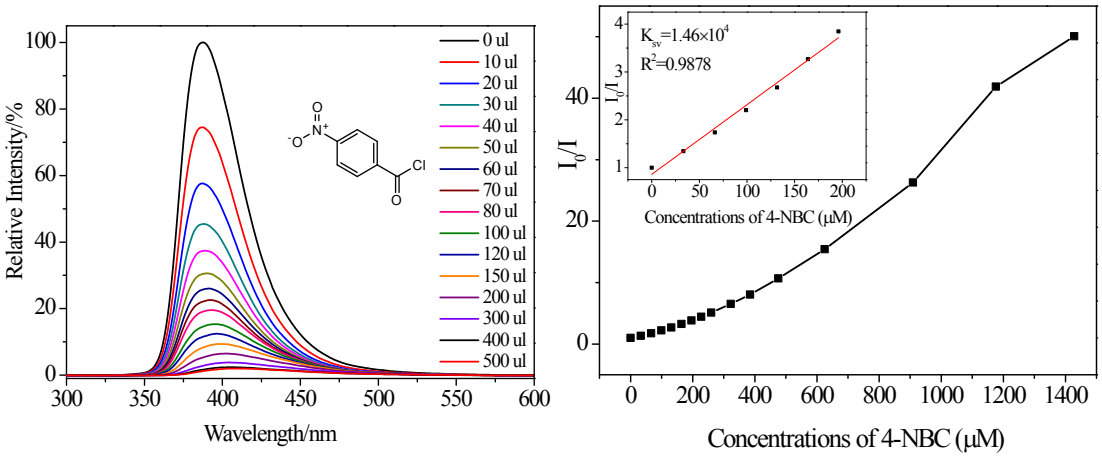
Relative Intensity/%
Wavelength/nm
0 ul
10 ul
20 ul
30 ul
40 ul
50 ul
60 ul
70 ul
80 ul
100 ul
120 ul
150 ul
200 ul
300 ul
400 ul
500 ul
Cl
K_{sv}=1.46×10^4
R^2=0.9878
I_0/I
Concentrations of 4-NBC (μM)

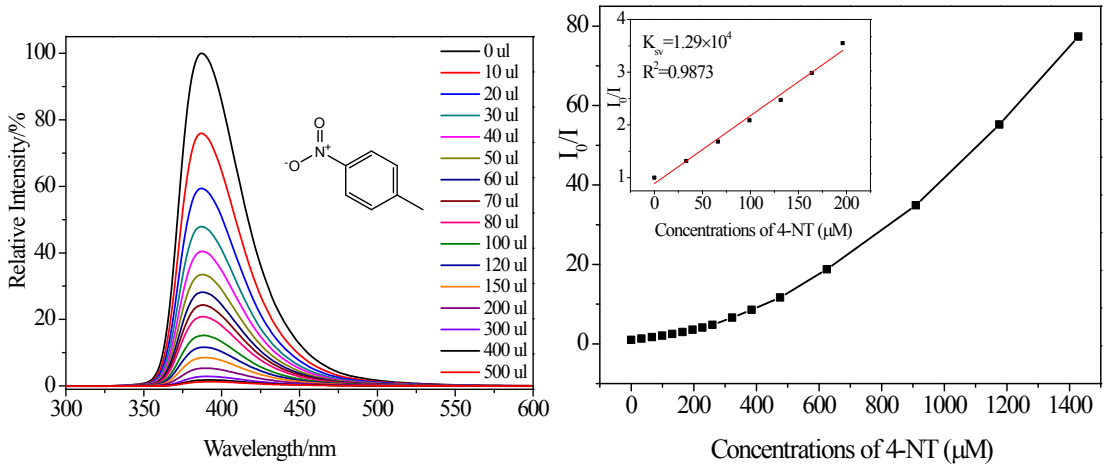
Relative Intensity/%
Wavelength/nm
0 ul
10 ul
20 ul
30 ul
40 ul
50 ul
60 ul
70 ul
80 ul
100 ul
120 ul
150 ul
200 ul
300 ul
400 ul
500 ul
K_{sv}=1.29×10^4
R^2=0.9873
I_0/I
Concentrations of 4-NT (μM)

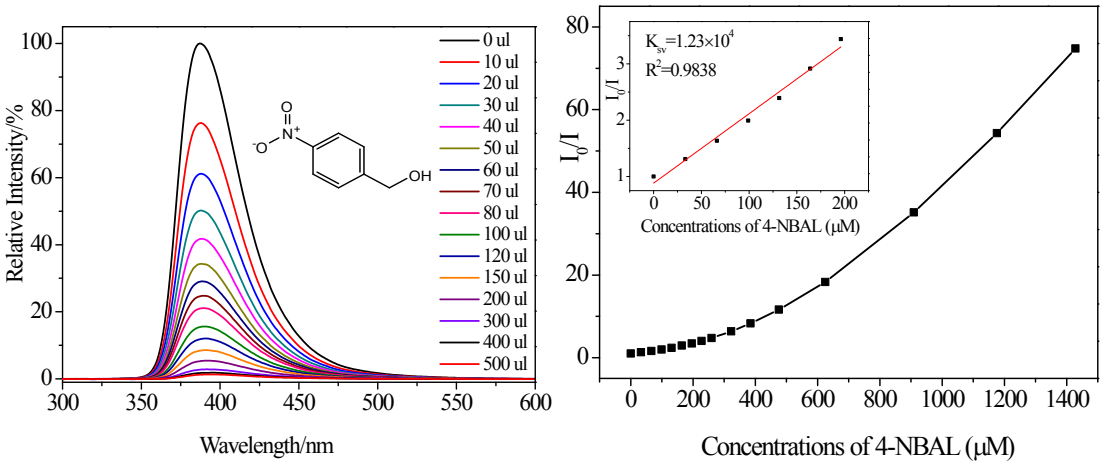
Relative Intensity/%
Wavelength/nm
0 ul
10 ul
20 ul
30 ul
40 ul
50 ul
60 ul
70 ul
80 ul
100 ul
120 ul
150 ul
200 ul
300 ul
400 ul
500 ul
OH
K_{sv}=1.23×10^4
R^2=0.9838
I_0/I
Concentrations of 4-NBAL (μM)

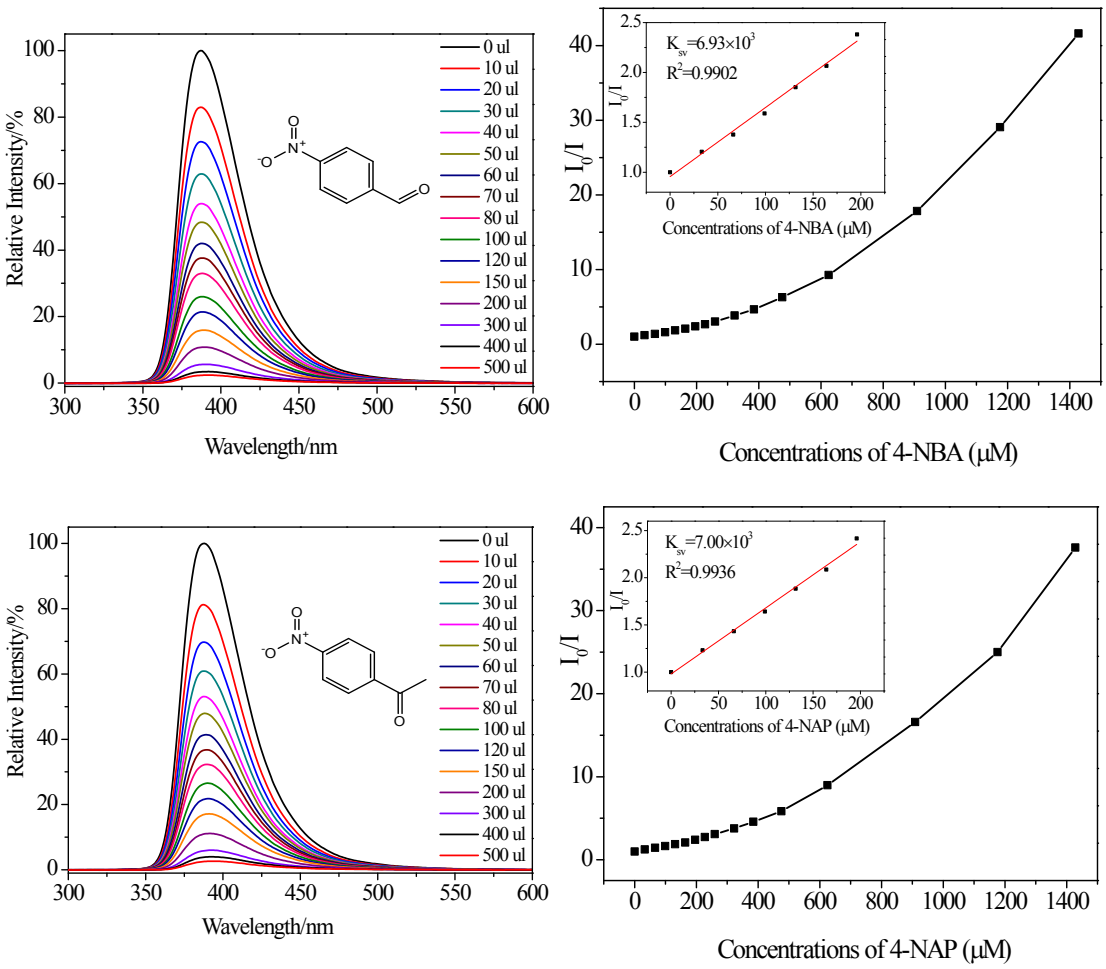

Fig. S11 Photoluminescence spectra and SV curves for **1** by gradual addition of 10^{-2} mol/L of various nitroaromatic compounds in DMF suspensions, the insets demonstrate the quenching linearity relationship at low concentrations of various nitroaromatic compounds.

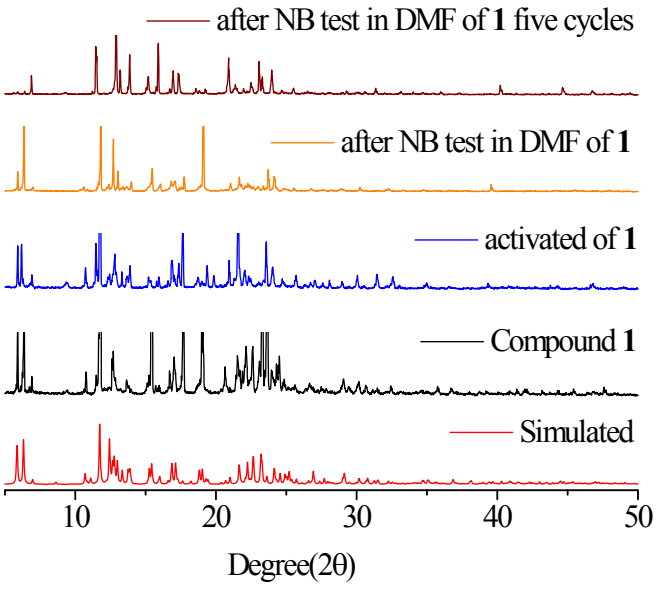

Fig. S12 Powder X-ray diffraction patterns of compound **1**, activated, after NB test in DMF and

after NB test in DMF five cycles.

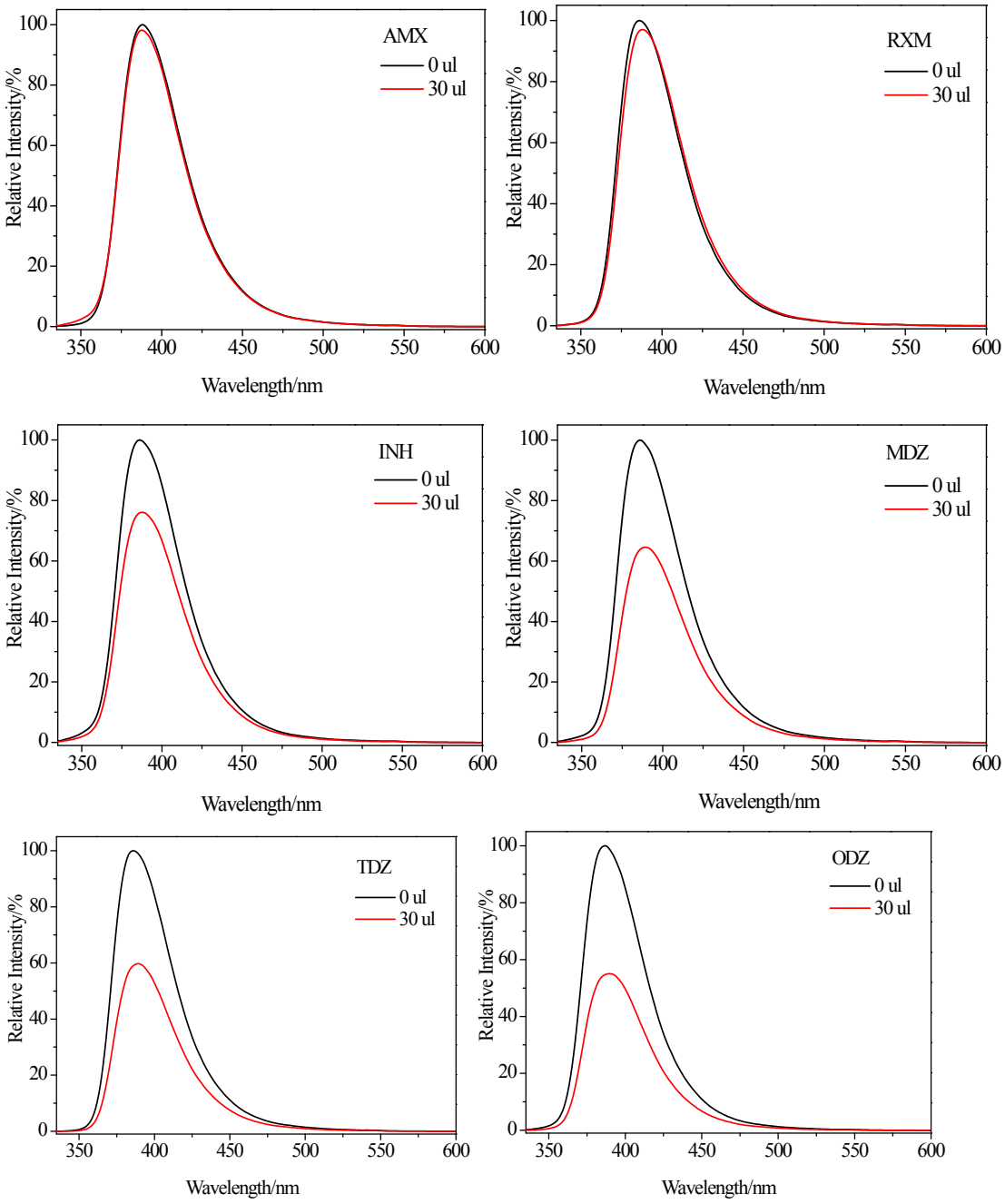

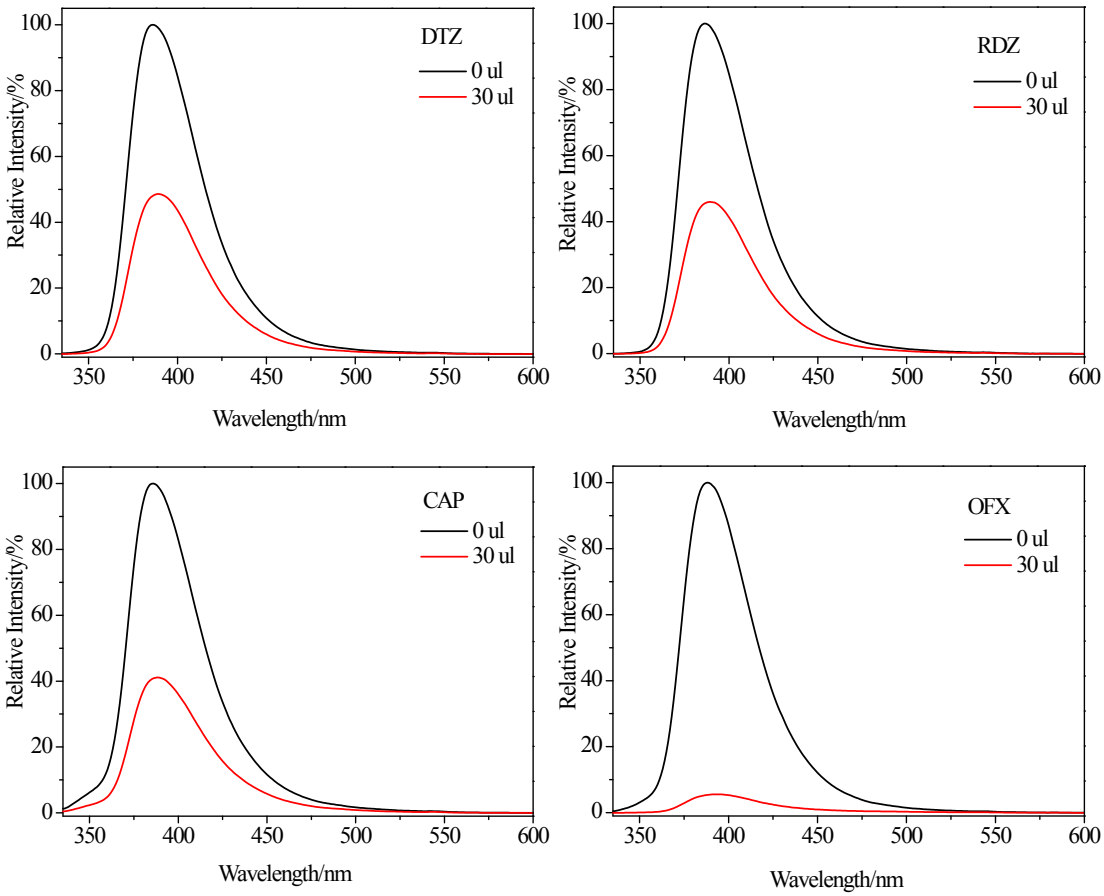

Fig. S13 The fluorescence spectra of compound **1** in DMF solution upon the addition of 10^{-2} mol/L of various antibiotics.

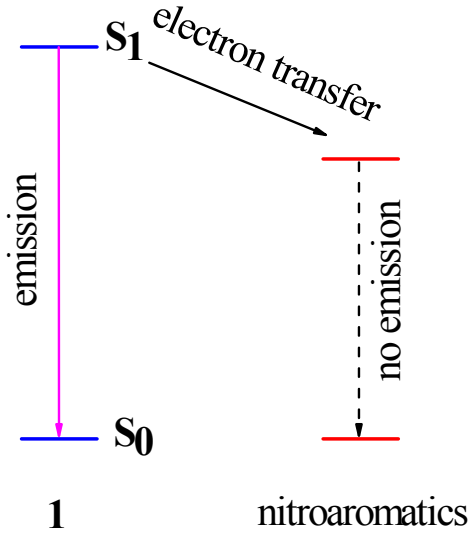

Fig. S14 Schematic representation of fluorescence emission and electron-transfer processes.

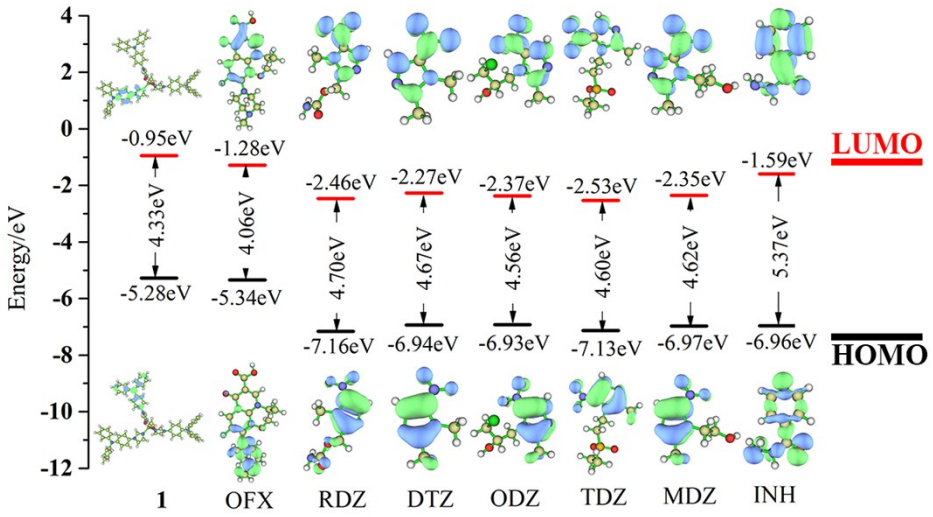

Fig. S15 HOMO and LUMO energy levels of compound **1** and antibiotics (The energy levels of frontier molecular orbitals were calculated by DFT at the level of B3LYP/6-31G*–SDD).

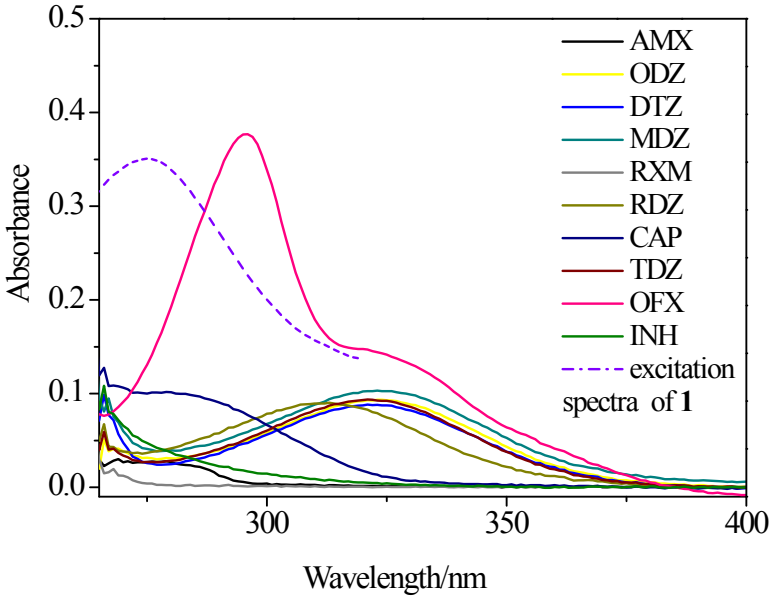

Fig. S16 The UV-Vis absorption spectra of various antibiotics and the excitation spectra of **1**.

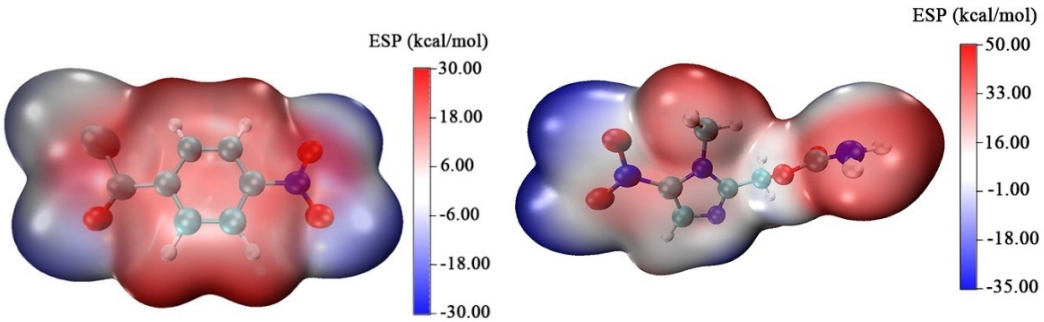

Fig. S17 ESP mapped molecular vdW surface of 4-NBC, RDZ.

Table S1 Crystallographic Data and Structure Refinement Details for **1** and **2.**

Compound	**1**	**2**
formula	$C_{61}H_{60}N_{16}O_{14}Zn_2$	$C_{34}H_{31}N_7O_7Zn$
formula weight	1371.99	715.03
crystal system	orthorhombic	monoclinic
space group	$P222_1$	$P2_1/c$
a (Å)	8.2598(6)	10.772(5)
b (Å)	13.9770(11)	30.453(14)
c (Å)	30.125(2)	10.404(5)
α (deg)	90	90
β (deg)	90	102.632(7)
γ (deg)	90	90
V (Å^3)	3477.9(5)	3330(3)
Z	2	4
D_c (g cm^{-3})	1.310	1.426
μ(Mo Ka)(mm^{-1})	0.76	0.80
F(000)	1420	1480
GOF	1.074	1.014
R(int)	0.056	0.099
R_1, wR_2 [$I > 2\sigma(I)$]	0.0597, 0.1303	0.0710, 0.1545
R_1, wR_2 (all data)	0.0733, 0.1336	0.1108, 0.1646

$R1=\Sigma||F_o|-|F_c||/\Sigma|F_o|$; $wR2=\{\Sigma[w(F_o^2-F_c^2)^2]/\Sigma[w(F_o^2)^2]\}^{1/2}$; where $w=1/[\sigma^2(F_o^2)+(aP)^2+bP]$, $P=(F_o^2+2F_c^2)/3$

Table S2 Selected bond lengths (Å) and angles (deg) for **1** and **2.**

Compound 1			
Zn1—N1	2.006(4)	Zn1—N3	1.976(4)
Zn1—N5	2.003(4)	Zn1—O1	2.095(3)
Zn1—O2	2.414(3)		
N3—Zn1—N5	112.08(16)	N3—Zn1—N1	108.43(16)
N5—Zn1—N1	103.48(16)	N3—Zn1—O1	108.04(14)
N5—Zn1—O1	128.87(14)	N1—Zn1—O1	92.29(15)
N3—Zn1—O2	96.89(14)	N5—Zn1—O2	89.08(14)
N1—Zn1—O2	144.38(14)	O1—Zn1—O2	55.41(12)
Compound 2			
Zn1—N1	1.987(4)	Zn1—N3	2.005(4)
Zn1—O1	1.942(4)	Zn1—O4	1.926(4)
O4—Zn1—O1	94.18(18)	O4—Zn1—N1	113.20(17)
O1—Zn1—N1	121.88(19)	O4—Zn1—N3	116.23(19)
O1—Zn1—N3	107.8(2)	N1—Zn1—N3	104.09(17)